The Astrophysical Journal, 570:557–572, 2002 May 10

UNDERSTANDING THE NATURE OF OPTICALLY FAINT RADIO SOURCES AND THEIR CONNECTION TO THE SUBMILLIMETER POPULATION

Scott C. Chapman,[1] Geraint F. Lewis,[2] Douglas Scott,[3] Colin Borys,[3] and Eric Richards[4]

Received 2001 August 16; accepted 2002 January 7

ABSTRACT

We present a sample of 43 submillimeter sources detected (at $>3\ \sigma$) drawn from our program to follow up optically faint radio sources with the Submillimeter Common User Bolometric Array (SCUBA) instrument. These sources already have associated radio and, in many cases, optical identifications, and many are also detected at 450 μm. We compare these with 12 submillimeter sources drawn from the literature, which were discovered in blank-field mapping campaigns but also have radio detections. We then use this total sample (55 sources) to study and model the evolution of dusty galaxies. A correlation is observed in the submillimeter/radio color-magnitude diagram (CMD), which can be modeled by strong luminosity evolution. The selection effects of the radio/optical preselection technique are determined from the models, and a corrected redshift distribution is constrained using a range of model assumptions. The temperature/redshift effects on the 450 μm detected subset of our sample are studied in relation to the models, and prospects for improved measurements in the shorter submillimeter wavelength windows (450 and 350 μm) are explored.

Subject headings: galaxies: evolution — galaxies: formation — galaxies: high-redshift — radio continuum: galaxies — submillimeter

1. INTRODUCTION

The advent of the Submillimeter Common User Bolometer Array (SCUBA) on the James Clerk Maxwell Telescope (JCMT) has spawned a new era of discovery in the submillimeter wave bands. Submillimeter luminous extragalactic sources were quickly uncovered (Smail, Ivison, & Blain 1997) as the possible high-redshift analogs to local ultraluminous infrared galaxies (ULIRGs). However, the population continues to be poorly understood, largely as a result of two observational difficulties. First, obtaining large samples of objects from SCUBA submillimeter mapping is an arduous process, whereby typically one to two sources are uncovered in a night's worth of integration on a blank piece of sky. Second, identifying secure detections at other wavelengths is tremendously difficult due to the positional uncertainty and large SCUBA beam size (15″) and the intrinsic faintness of most sources at all other wavelengths.

The tight correlation observed locally between thermal far-infrared (far-IR) emission and synchrotron radio emission (Helou et al. 1985; Condon 1992) suggests a possibility for identifying the submillimeter sources. The positional accuracy and small beam sizes of large radio interferometers such as the VLA can act as a surrogate to the submillimeter, allowing precise identifications at other wavelengths. Smail et al. (2000) demonstrated that a significant fraction of their submillimeter sources could be detected in the radio. However, reaching the radio depths required to detect the submillimeter sources is not trivial. Even the deepest radio map yet obtained, a 100 hr VLA integration at 1.4 GHz in the selected survey area (SSA) 13 survey region (Fomalont et al. 2002) cannot detect all the bright submillimeter sources found in this field (Barger et al. 2001a). At this depth ($S_{1.4\,\mathrm{GHz}} = 20\ \mu$Jy) submillimeter sources with warm ($\sim$50 K) dust and luminosities similar to the local ULIRG, Arp 220, will likely be missed at $z \gtrsim 3$. Colder sources would be missed at even lower redshifts (Blain 1999).

Putting aside the precise form of the radio/submillimeter overlap, deep radio observations have emerged as an efficient means to preselect high-redshift, submillimeter sources (Barger, Cowie, & Richards 2000a, hereafter BCR; Chapman et al. 2001a, hereafter C01). This effectively circumvents the time constraint for obtaining large samples of objects with the present-generation submillimeter imaging instruments, SCUBA (Holland et al. 1999) and MAMBO (Bertoldi et al. 2000). These surveys (BCR, C01) have used the bimodal break in the apparent optical magnitudes of radio source identifications lying at $I \sim 24$ (Richards et al. 1999), selecting only the relatively faint sources for submillimeter follow-up—the optically faint radio sources (OFRS). While the entire blank-field submillimeter population (e.g., Smail et al. 2001) is not selected in this manner, a significant percentage of the source counts are recovered ($\sim$70%; BCR, C01). The key advantage, however, is that the optical and radio properties of the sources are known with certainty, with the high-resolution radio providing morphological information for studying the types of galaxies in the submillimeter population (Richards 2000). The challenge is to understand the selection function sufficiently to exploit the rich information gleaned by the large samples of submillimeter sources uncovered in this manner.

In this paper, we investigate the evolutionary behavior of the submillimeter population of galaxies, constrained by the correlations observed in a large sample selected using the radio. We develop models to describe the form of the evolution and study the model-implied radio selection function. The detailed multiwavelength properties of this large sample of radio-selected submillimeter sources are presented elsewhere (Chapman et al. 2002, in preparation; Barger et al. 2001b). We give only a brief description in § 2, and show

[1] California Institute of Technology, Pasadena, CA 91125; schapman@irastro.caltech.edu.
[2] Anglo-Australian Observatory, P.O. Box 296, Epping, NSW 1710, Australia.
[3] Department of Physics and Astronomy, University of British Columbia, BC V6T 1Z1, Canada.
[4] Department of Physics and Astronomy, University of Alabama, Huntsville, AL 85287.

color-magnitude diagrams (CMDs) in § 3. We adopt two modeling approaches. In § 4, we take the local *IRAS* bright galaxy sample and evolve individual sources according to prescriptions that are able to fit the SCUBA counts (e.g., Blain et al. 1999a) and the far-IR background (Puget et al. 1996; Fixsen et al. 1998). In § 5, we adopt a Monte Carlo approach, drawing luminous infrared galaxies randomly from evolving distributions. We use these models to better understand the range in properties sampled by the radio preselected submillimeter galaxy population in § 6. We then discuss shorter wavelength submillimeter detections in § 7 and consider wider implications and future directions in § 8.

2. SAMPLE DEFINITION

We draw on the large number of submillimeter sources cataloged and described in Chapman et al. (2002, in preparation) and Barger et al. (2001b), which were obtained through SCUBA follow-up to radio sources in the extended Hubble Deep Field (HDF) and the Hawaii SSA 13 survey field. The main sample consists of 43 sources detected at 850 μm above 3 times the rms, corresponding to about 5 mJy. Twenty of these were already presented in BCR and C01. The sources were observed in SCUBA photometry mode, keeping the source on a bolometer at all times (3-bolometer chopping; C01) in order to go deeper than making a fully sampled map of the field. Targets were selected to be optically faint, with no optical source having flux $I < 24$ being coincident with the radio position.

Several of these sources have radio/optical astrometry which is difficult to reconcile with radio source centroids offset from relatively bright optical sources by $0\farcs5$ to $1\farcs5$. In C01, we assumed that six such sources were optically fainter than $I > 25$ (three detected in the submillimeter and three undetected). Further statistical analysis and a more precise astrometric solution now suggest that these optically brighter sources *are* the likely counterparts to the radio sources. Submillimeter follow-up of radio sources subsequent to the C01 study has extended the sample into optically brighter sources as described in Chapman et al. (2002a). Such endeavors have continued to uncover submillimeter luminous sources, albeit at a lower recovery rate than the $I > 25$ samples. We estimate that the submillimeter recovery rate for radio sources with $I > 24$ is 38%.

The submillimeter follow-up to radio sources leaves a large *undetected* sample, with an implied $S_{850} < 5$ mJy. This begs the question as to the nature of these sources. As discussed in C01, this undetected radio sample has significant submillimeter flux on average, even if they are too faint to detect individually. Since there is no significant difference in the radio flux distribution between the submillimeter detected and undetected OFRS samples, one interpretation is that they are a lower redshift continuation of our detected sample (intrinsically less radio-luminous and harder to detect with SCUBA). However, we do not discount the possibility raised in Richards et al. (1999) that these sources could be high-redshift, radio-loud active galactic nuclei (AGNs). Some fraction of them could also be displaced radio lobes from other radio sources.

A simple inspection of the spectral energy distribution (SED) for the ULIRG Arp 220 suggests that the deep VLA maps used both to select the OFRS for SCUBA follow-up and to attempt identification of submillimeter blank-field surveys ($\sim$40 μJy completeness) will not detect a galaxy with twice the luminosity of Arp 220 (beyond $z \sim 3\left[S_{850\,\mu\mathrm{m}} \sim 5\right]$ mJy). However, the submillimeter selection function suggests that sources typically detectable by SCUBA should lie mostly at $z > 1$ (Blain et al. 1999b). Thus, the radio-identified submillimeter population suggests a redshift range spanning $z \sim 1$–3.

We also collected submillimeter sources with radio identifications from the literature in order to compare the properties of sources drawn from blank fields to our OFRS selected submillimeter sources. Seven sources from the Smail et al. (2001) catalog and five from Eales et al. (2000) were identified in the radio and can thus be compared with our sample. Smail et al. (2001) have suggested optical counterparts for their objects, four of which are optically fainter than $I > 24$, while three lie between $21 < I < 24$.

3. THE SUBMILLIMETER/RADIO CMD

A favorable situation exists for studying high-redshift sources in the submillimeter wave band: for submillimeter sources lying at redshifts greater than about 1, we can use the submillimeter flux alone to estimate the overall luminosity, only weakly dependent on redshift because of the offsetting effects of the steep positive spectral index in the submillimeter and cosmological dimming. The negative spectral index in the radio further implies that the submillimeter/radio ratio can be used as a rough redshift indicator (Carilli & Yun 1999, 2000; Dunne et al. 2000a; BCR), effectively tracing the trough in the SED formed by the opposing spectral indices.

The flat luminosity-redshift relation implies that any trends observed in the ratio of submillimeter/radio as a function of submillimeter flux must be a result of evolutionary effects. Of immediate interest for our sample is therefore to analyze the $S_{850\,\mu\mathrm{m}}/S_{1.4\,\mathrm{GHz}}$ versus $S_{850\,\mu\mathrm{m}}$ plane—essentially a submillimeter/radio CMD. For sources at $z > 1$, and in the absence of varying dust effects, such a CMD can be interpreted simply in terms of redshift (y-axis) and luminosity (x-axis). However, the redshift estimated in this manner is degenerate with dust temperature (Blain 2000), and it is only the quantity $(1 + z)/T_d$ that is truly constrained by the submillimeter/radio ratio. This increases the impetus to study the CMD in order to assess any obvious trends of this redshift/temperature indicator with submillimeter flux density.

In Figure 1, we present the submillimeter/radio CMD for the total submillimeter observed OFRS sample. Solid circles represent radio sources detected with $\gtrsim 3\ \sigma$ significance at 850 μm. An error bar representative of the root mean square (rms) error for the detected sample is shown in the lower right corner. Solid circles show an additional 24 sources from our sample which have $\gtrsim 2\ \sigma$ significance at 850 μm. While we do not consider these robust detections, a large fraction will be real submillimeter sources, and the average properties of this *marginally* detected sample will help extend the statistical properties of OFRSs to fainter fluxes. Crosses represent radio sources with $<2\ \sigma$ significance at 850 μm, where sources with negative submillimeter flux density have been arbitrarily plotted at $S_{850} = 0.3$ mJy.

In interpreting Figure 1, we caution that our sample is only complete at a flux limit of $S_{850} \gtrsim 5$ mJy, resulting in accurate distributions in the CMD plane only for these brightest sources. Nevertheless, an apparent correlation is seen, whereby an increasing ratio of 850 μm flux to 1.4 GHz

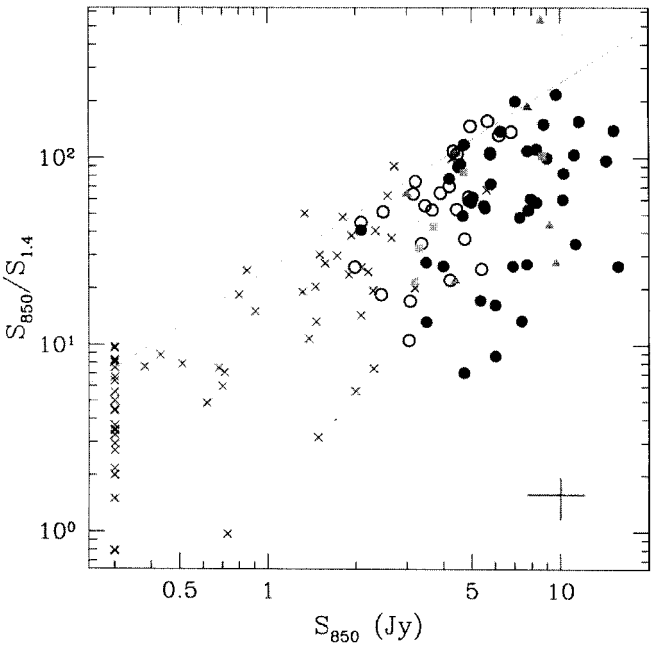

FIG. 1.—Radio $S_{850\,\mu m}$ color-magnitude diagram. Solid circles are radio sources detected with $\gtrsim 3\,\sigma$ significance at 850 μm, while open circles are an additional sample of sources marginally detected at $>2\,\sigma$. The error bar in the lower right is representative of the detected sample. Crosses show radio sources with $<2\,\sigma$ significance at 850 μm, where those with observationally estimated fluxes which are negative being plotted at $S_{850} = 0.3$ mJy. We also plot the submillimeter sources with radio counterparts from Smail et al. (2001) and Eales et al. (2000) as seven triangles and five squares, respectively. The typical radio flux limit of the sample is shown as a dashed line; the two sources lying above the line were selected from the deeper SSA 13 radio field. A correlation is apparent in the data, but this is largely defined by the upper envelope of the radio sensitivity cutoff.

flux scales with increasing S_{850}. This correlation plausibly extends into the regime of radio sources with $<3\,\sigma$ significance in the submillimeter (*open circles and crosses*). However, the absence of sources in the upper left corner of the diagram is largely the result of the radio flux limit of the survey, which we represent with a dashed line. Note that the two $>3\,\sigma$ sources lying above the line were selected from the deeper SSA 13 radio field. On the other hand, the dearth of sources in the lower right of Figure 1, compared with the high density of sources in the upper right, must be a true evolutionary effect.

As a comparison with other studies, we also plot in Figure 1 the submillimeter sources with radio counterparts from the catalogs of Smail et al. (2001) and Eales et al. (2000) as seven triangles and five squares, respectively. Of interest is the fact that these sources lie scattered around the complete CMD area probed by our OFRS sample, with no obvious bias for the optically brighter members. It is therefore plausible that these sources may trace the same evolutionary trends uncovered by our OFRS population, irrespective of the optical emission. We return to this point later.

Note that all sources presented in the diagram are robustly detected in the radio and are likely to be relatively high star formation rate galaxies, as noted in § 2 above, whether or not we were able to obtain secure submillimeter detections. We can thus study with confidence the CMD at the bright end. However, a more detailed assessment of the population lying in the 1–5 mJy range will require additional, deeper submillimeter measurements, which would provide significant leverage of the CMD correlation to fainter submillimeter flux densities.

4. LOCAL CMD RELATIONS AND A SIMPLE PICTURE OF EVOLUTION

To better understand the intrinsic scatter and correlations present in the submillimeter/radio population at higher redshifts, we examine the local infrared luminous population in the radio and at submillimeter-to-far–IR wavelengths. We present a sample of 19 objects from the *IRAS* bright galaxy sample (BGS) which have been measured at 850 and 450 μm (Dunne & Eales 2001) and in the radio (Condon et al. 1996). We plot them in the CMD plane (Fig. 2*a*) as well as color-color diagrams consisting of either S_{100}/S_{850} or S_{450}/S_{850} versus $S_{850}/S_{1.4\,\mathrm{GHz}}$ (Figs. 2*b*, 2*c*). For the range of likely redshifts of the SCUBA sources in this study ($z \sim 1$–4), the 850 μm band will remain a probe of the Raleigh-Jeans graybody tail of the SED. However, the observed 450 μm band will sample a very different part of the SED at higher redshifts, comparable to $\sim$100 μm locally.

The 850 μm/radio CMD reflects the intrinsic scatter in the far-IR/radio relation, coupled with the dispersion from dust temperatures and emissivities as well as measurement uncertainties. The measured scatter of 0.2 dex in 850 μm/radio (Table 1) is close to that found for the far-IR/radio (Helou et al. 1985).

The 450 μm/850 μm CMD shows a flat relation, representing a fairly constant and cool dust temperature component ($\sim$20 K), as discussed in Dunne & Eales (2001). The 100 μm/850 μm and 60 μm/100 μm CMDs, however, show a rather large scatter, indicative of a range in warmer ($\sim$40 K) dust properties found in this local infrared luminous sample.

The local galaxy color-color relations, using the 450 μm/850 μm versus 850 μm/radio, continue to reflect the apparent constancy of the cool dust properties of this sample. The color-color relation using the local 100 μm band, however, now forms a strong correlation (compare Figs. 2*a*, 2*b*), reflecting the effect of dust temperature and emissivity variations on both the 100 μm/850 μm and the 850 μm/radio. This arises since the change in temperature effectively changes the total far-IR luminosity for a fixed 850 μm measurement, and thus changes the correlation of far-IR/radio. The 60 μm band is similar to the 100 μm but exhibits larger scatter as it lies beyond the graybody peak and, hence, has contributions from a range of dust components.

While 19 objects is a small sample from which to establish local correlations, a larger sample exists for *IRAS* galaxies measured only at 850 μm Dunne et al. (2000b). CCDs for this larger *IRAS* sample are presented in Figure 2*c*. The steep negative correlations in the 100 μm/850 μm and 60 μm/850 μm diagrams are still observed, with similar scatter as in the 19-object sample. For reference, we list the scatter and slope of all these local correlations in Table 1

These correlations may arise due to sources with the highest dust temperatures (and hence 100 μm/850 μm, 60 μm/100 μm ratios), having effectively have lower far-IR fluxes for galaxies in this limited range of L_{850}. The 850 μm/1.4 GHz ratio, scaling inversely with far-IR, is therefore also lower. The 850 μm/1.4 GHz correlation from the SED template catalog of Dale et al. (2001a, 2001b) suggests that the more quiescent galaxies have a significantly greater 850 μm/1.4 GHz ratio than active IR-luminous star-forming gal-

TABLE 1
LOCAL *IRAS* GALAXY RADIO/SUBMILLIMETER/FAR-IR CORRELATIONS

Relation	Slope[a]	Log (y-intercept)[b]	Scatter (dex)[c]
100 μm/850 μm vs. 850 μm	0.13	0.97	0.16
60 μm/850 μm vs. 850 μm	0.27	−0.45	0.26
450 μm/850 μm vs. 850 μm	−0.07	1.45	0.07
850 μm/1.4 GHz vs. 850 μm	−0.08	1.04	0.19
100 μm/850 μm vs. 850 μm/1.4 GHz	−0.63	2.30	0.12
60 μm/850 μm vs. 850 μm/1.4 GHz	−1.03	2.25	0.21
450 μm/850 μm vs. 850 μm/1.4 GHz	0.06	0.87	0.07
100 μm/850 μm vs. 850 μm/1.4 GHz[d]	−0.48	2.23	0.13
60 μm/850 μm vs. 850 μm/1.4 GHz[d]	−0.66	2.08	0.22

[a] Power-law slope index $S_\nu \propto \nu^\alpha$.
[b] Log of the power-law coefficient A in $S_\nu = A\nu^\alpha$.
[c] Scatter in power-law fit to the data measured in dex.
[d] Fits to 121 galaxies having only 850 μm flux densities from Dunne et al. 2000a rather than the 19 from Dunne & Eales 2001, with additional 450 μm measurements.

REFERENCES.—Data taken from Dunne et al. 2000a and Dunne & Eales 2001.

axies (as expected, since the quiescent galaxies have colder dust). By redshifting the SEDs, we can anticipate the effect of this monotonic scaling of 850 μm/1.4 GHz with galaxy IR luminosity on our high-z CMD and color-color diagram relations. Local infrared sources can thus be understood as correlating tightly in color-color space, due to the effect of dust properties and star formation on both the radio and the far-IR windows, leaving the 850 μm and 450 μm flux densities relatively constant. This behavior is modeled in detail in Dale et al. (2001a, 2001b).

In the absence of evolution, tracing sources to higher redshifts would lead to results following the trend discussed above: the sources retain the same observed flux density while increasing in 850 μm/radio as a function of redshift (Fig. 3*a*). If we propose instead that a population of IR-luminous objects undergoes a strong luminosity evolution of the form $(1+z)^4$ out to $z = 3$, turning over to $(1+z)^{-4}$ to $z = 6$ (Fig. 3*b*), then the local sources move along the direction suggested in our observed SCUBA source sample (Fig. 1). The CMD trend can be understood naturally in terms of luminosity evolution: more luminous objects occur at higher redshifts, leaving the lower right corner largely empty. Note that here, and in what follows, we explicitly use an Einstein–de Sitter cosmology.

The source density in comoving coordinates is fixed since we have simply evolved the local sample of sources in luminosity. The $z = 0$ sources (*point symbols*, Fig. 3) would therefore only be detected in an enormous survey field. A dashed line represents the radio sensitivity limit of the VLA for ~50 hr integrations at 1.4 GHz. Sources beyond the peak in our luminosity evolution function quickly traverse this radio limit and would not be detected either. The luminosity range of these sources spans $\log(L_{\rm far-IR}) = 10$–12. For the luminosity evolution invoked in our model, all the submillimeter sources could evolve from such a local sample and be at redshifts 1–4.

The local source sample represents an average dust temperature of $T_d = 36$ K (Dunne et al. 2000a). In Figure 3*c*, we also evolve a subset of the local sources with cooler ($T_d = 25$ K; *triangles*) and hotter ($T_d = 50$ K; *open circles*) dust temperatures, keeping the 850 μm luminosity fixed. As demonstrated in Dale et al. (2001a, 2001b), this is equivalent to fixing the mid-IR luminosity (~10 μm) but results in proportionately higher far-IR (hot dust) or lower far-IR (cool dust) sources. Therefore, a sample of equivalently far-IR luminous sources with colder dust temperatures will be detected by SCUBA at much lower redshifts, and a less extreme luminosity evolution would be required to generate sources which lie in our submillimeter detection window $S_{850} > 5$ mJy. The effect of moving to a flat $\Lambda = 0.7$ cosmology, however, is to introduce a slope to the CMD which also has to be countered with luminosity evolution or colder sources to maintain sources in our detection window. However, the evolutionary effects are sufficiently strong that the precise cosmology adopted is relatively unimportant.

5. MODELING THE EVOLVING CMD RELATIONS

We now embark on more comprehensive models of our submillimeter/radio CMD and the trends observed in the previous sections. Our aim will be to simulate the properties of our data sample using a Monte Carlo approach and to use this to focus on the evolutionary trends implied by the SCUBA data for the OFRS sample. The data we have do not justify embarking upon a detailed fitting of various model parameters. Rather, we look at some examples of models which are motivated by fitting what is already known about local ULIRGs and distant SCUBA sources, and using these examples, try to draw general conclusions. We start with simple step-by-step assumptions about the population and progress to more involved and (hopefully) realistic effects, taking careful note of the changes in the resulting CMD.

Monte Carlo simulations of the 850 μm/1.4 GHz CMD are first attempted by assuming a population of Arp 220-like SEDs, equivalent in the far-IR/submillimeter regime to a graybody with dust temperature $T_d = 50$ K and emissivity $\beta = 1.5$. Figure 4*a* depicts an ensemble of such objects in the CMD, all having the same luminosity (approximately twice that of Arp 220). The sources follow a Gaussian redshift distribution (indicated in the insets in Fig. 4) matched to the spectroscopically estimated distribution of Barger et al. (1999), thought to be plausible in light of recent Keck redshift measurements for submillimeter sources (Chapman et

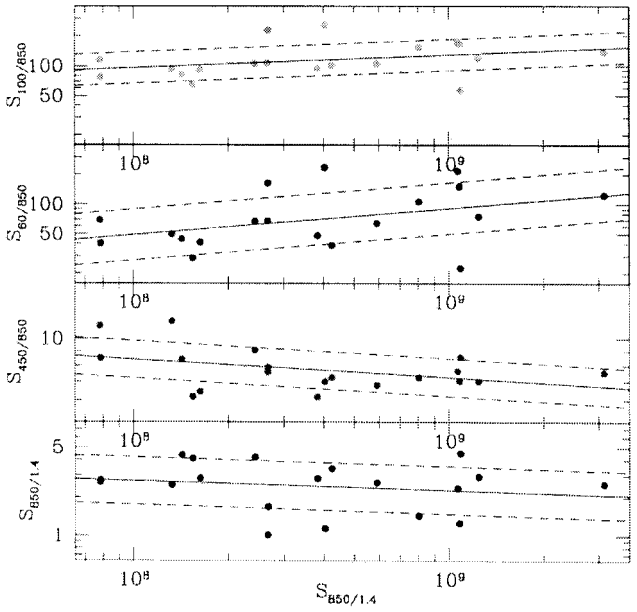

FIG. 2*a*

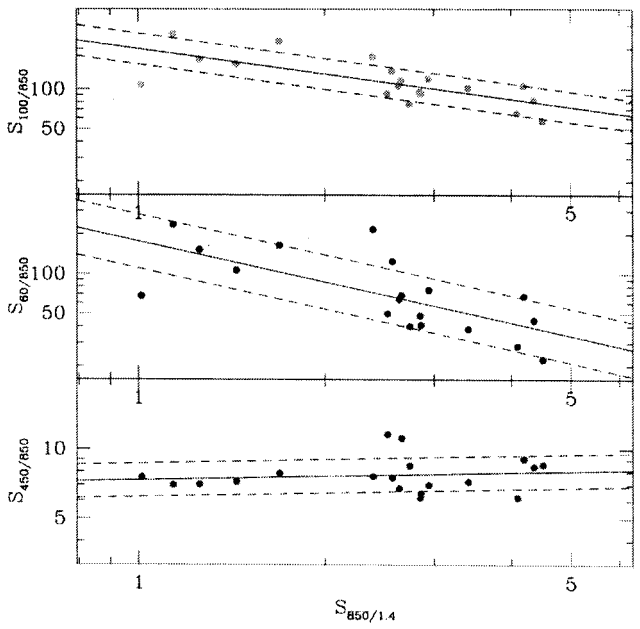

FIG. 2*b*

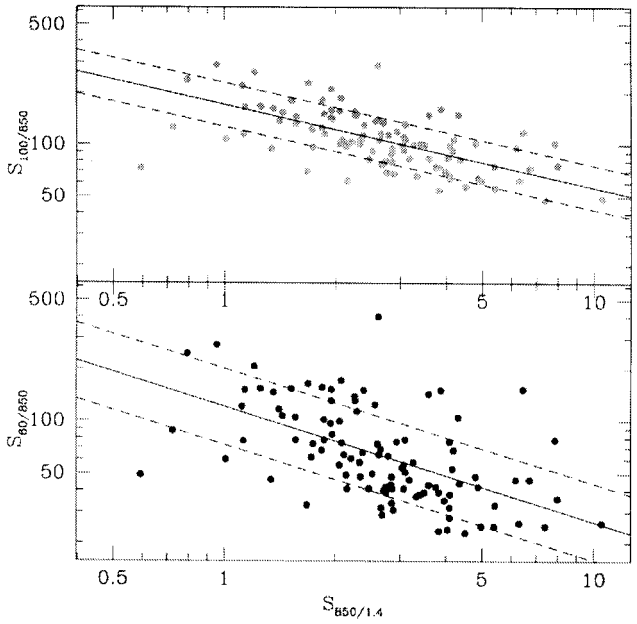

FIG. 2*c*

FIG. 2.—Local CMD and color-color relations for *IRAS* luminous galaxies. (*a*) CMDs for 19 galaxies observed at 850 and 450 μm by Dunne & Eales (2001), with L_{850} in units of $L_{\odot}$. Dashed lines represent the scatter about the best fitted relations (*solid lines*). (*b*) Color-color diagrams for these same 19 galaxies. Rather steep power-law correlations are observed in the 100 μm/850 μm and 60 μm/850 μm vs. 850 μm/1.4 GHz diagrams (with indices -0.63 and -1.03, respectively), while the 450 μm/850 μm relation remains flat. (*c*) Color-color diagrams for the larger *IRAS* sample from Dunne et al. (2000a), having only 850 μm follow-up.

al. 2002b). The sources are color-coded by redshift as described in the figure caption and represent density evolution of a single luminosity of source. This is effectively the opposite hypothesis to our toy model above, where the source density per comoving volume remained constant for all time but evolved in luminosity. The corresponding track then traces this characteristic submillimeter galaxy as a function of redshift through the CMD. Note that beyond $z \sim 1$, the source is observed with approximately the same 850 μm flux density for the adopted $\Omega_M = 1$ cosmology, reflecting the favorable submillimeter *K*-correction described above. However, redshifts map monotonically onto the 850 μm/1.4 GHz axis.

Since we know the local scatter in the 850 μm/1.4 GHz relation (as discussed in § 4, see also Helou et al. 1985; Yun, Reddy, & Condon 2001), we can introduce the assumption that this scatter remains constant and applies at all redshifts. We describe the relation as a Gaussian in the 850 μm/1.4 GHz ratio with an rms scatter of 0.2 dex. The effect of the scatter of this relation on the CMD distribution is shown in Figure 4*b*, distributing the single luminosity submillimeter family vertically. Without spectroscopic measurements, our

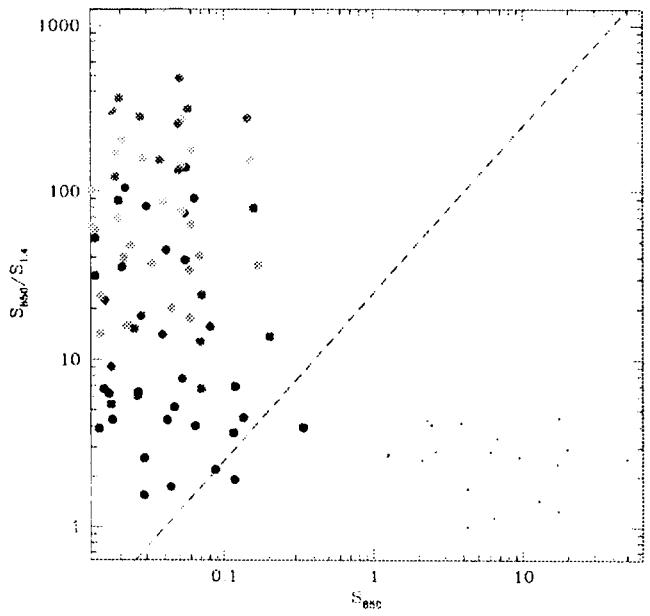

FIG. 3*a*

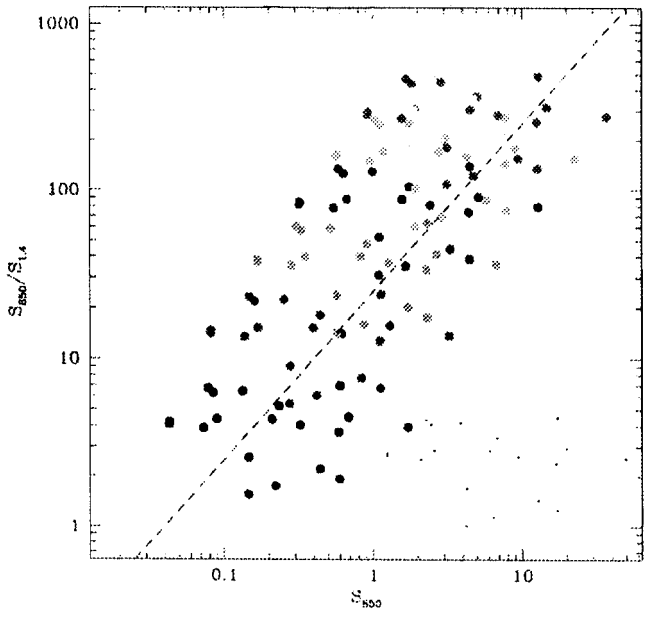

FIG. 3*b*

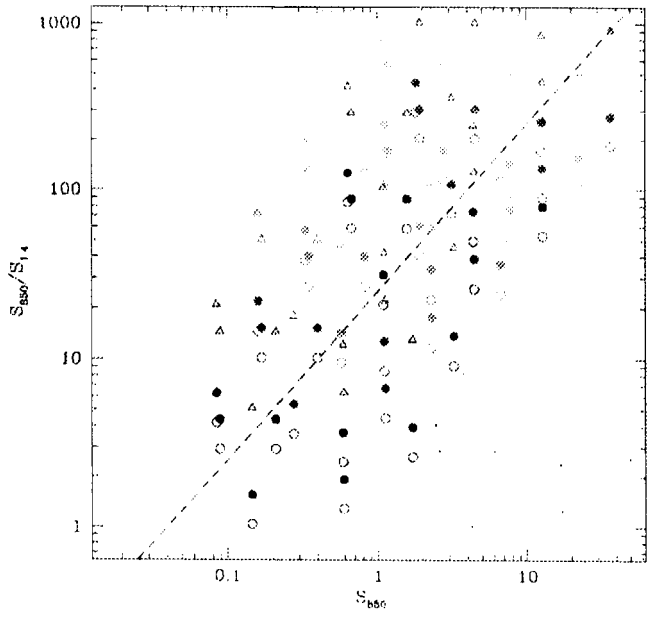

FIG. 3*c*

FIG. 3.—(*a*) Nineteen *IRAS* sources from Dunne & Eales (2001), shown at $z = 0$ by the points, have been redshifted as indicated by circles. Flux densities are calculated using the locally estimated luminosities using an $\Omega_M = 1.0$ cosmology. Beyond $z \simeq 1$, the sources retain approximately the same observed flux density, while increasing in 850 μm/radio as a function of redshift (i.e., moving vertically on the plot). (*b*) Evolution of the galaxies in luminosity, scaling by $(1 + z)^4$ out to $z = 3$, in an attempt to match our observed CMD from Fig. 1. Conversion from luminosity to flux density space results in the sources traveling roughly along the suggested CMD correlation, but then turning above our radio limit (*dashed line*) beyond the peak in the adopted luminosity evolution at $z = 3$. (*c*) Evolution of a subset of the local sources with cooler ($T_d = 25$ K; *triangles*), medium ($T_d = 36$ K; *solid circles*, the mean dust temperature from Dunne et al. 2000a), and hotter ($T_d = 45$ K; *open circles*) dust temperatures. The 850 μm luminosity is kept fixed here.

current data cannot constrain the true evolution in the far-IR/radio correlation. Such information will have to await future redshift surveys of radio and submillimeter detected sources (e.g., Chapman et al. 2002b). At the moment, assuming it is the same as the local relation is about the best that can be done.

We can alternatively impose a luminosity distribution on our ULIRG population, as represented in Figure 4*c*. The bright SCUBA counts at 850 μm are well fitted by a power law (e.g., Barger et al. 1999) and, hence, we first adopt a constant power law for our luminosity functions over all redshifts (*lower insets*, Fig. 4). This is probably a reasonable assumption for the bright submillimeter sources considered here. This therefore represents a null hypothesis for luminosity evolution. At this point, our radio survey completeness of 40 μJy imposes a diagonal cut on the sources from the upper left corner of the CMD.

We can then combine both the far-IR/radio scatter and luminosity function to create a candidate scenario for the CMD relation, as shown in Figure 4*d*. Scatter in radio/far-

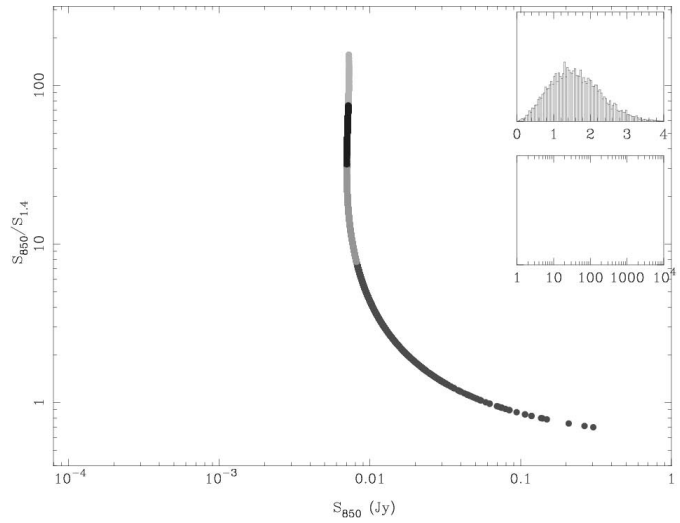

FIG. 4*a*

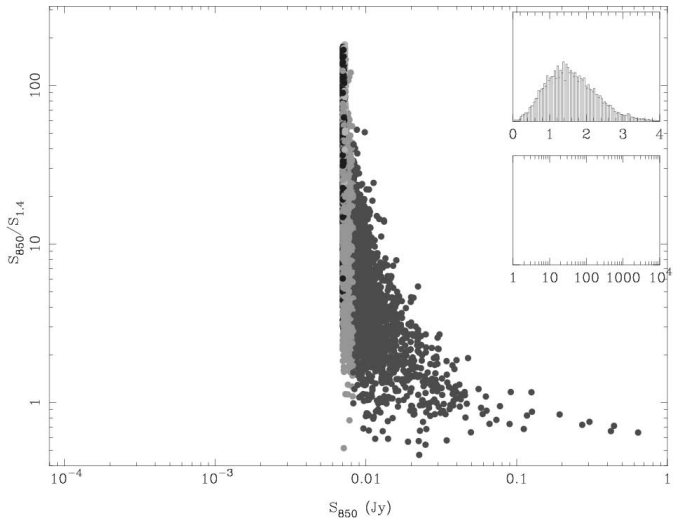

FIG. 4*b*

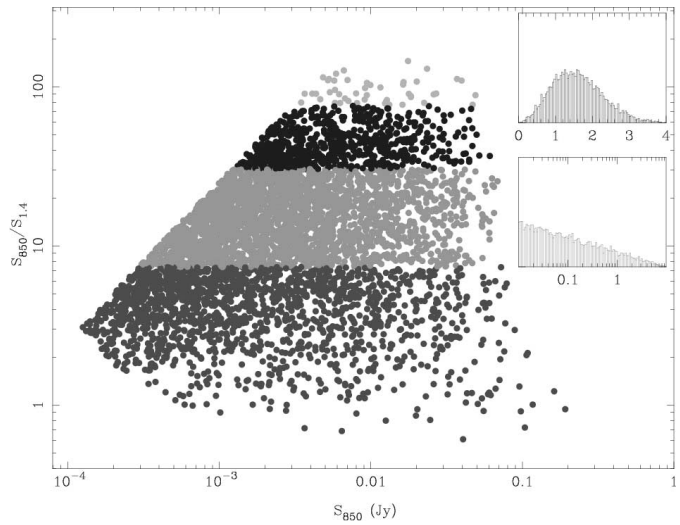

FIG. 4*c*

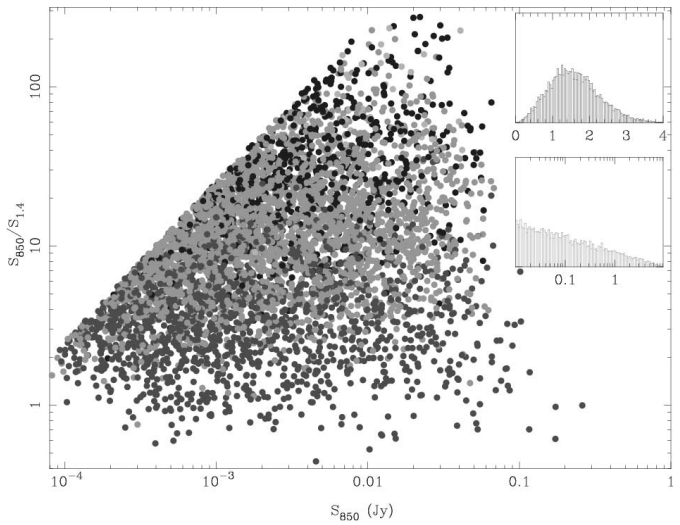

FIG. 4*d*

FIG. 4.—Monte Carlo simulations of the 850 μm/1.4 GHz CMD, showing the null hypothesis for pure luminosity evolution. (*a*) Population of ULIRG galaxies with about twice the luminosity of Arp 220 are plotted following a Gaussian redshift distribution (*first inset*). Gray-scale bands correspond to $z > 3$, $2 < z < 3$, $1 < z < 2$, and $z < 1$, respectively. The corresponding track through the CMB shows the redshift spread of galaxies of fixed luminosity and SED. This becomes vertical at high z, but redshifts are mapped one-to-one onto a specific value of $S_{850}/S_{1.4}$. (*b*) Spread in the $S_{850}/S_{1.4}$ ratio, corresponding to the locally observed scatter as measured in Table 1. (*c*) Imposing a luminosity distribution on our ULIRG population, represented here simply as a power law (*second inset*), is probably a reasonable assumption for the bright sources considered here. At this point, the radio survey limit imposes a diagonal cut out of the upper left corner of the CMD. (*d*) Effects of redshift distribution, submillimeter/radio scatter, and luminosity function are combined to create a possible realization for the CMD relation. This scenario is clearly incompatible with our observed CMD.

IR relation has a skewed effect on the data compared to Figure 4*c*, in the sense of pulling more high-redshift objects downward in the diagram. This can be understood as resulting from a selection bias associated with our radio threshold.

This scenario is clearly incompatible with our observed CMD, failing to reproduce the dearth of sources in the lower right corner of Figure 1. What can we learn from the failure of this picture to help understand how to recover the observational trend in the CMD? First, the model consisted of no luminosity evolution with redshift and a mild number density evolution governed by the imposed redshift distribution. As noted by Blain et al. (1999b, 1999c), the extremely strong density evolution required to fit the 850 μm counts (following a $[1 + z]^6$ form) will quickly overproduce the far-IR background. Boosting our present redshift distribution is not a viable modeling route.

The key to the problem lies in removing sources (which do not exist at all in the observations, despite our apparent sensitivity to them) from the lower right corner. As discussed in the previous section, with our toy evolution of a local sample of *IRAS* galaxies, a reasonably strong luminosity evolution on its own is able to reproduce the general trend of the CMD. Several authors have recently modeled the evolution of dusty galaxies using pure luminosity evolution, reproducing the observed counts and backgrounds at both far-IR and submillimeter wavelengths (e.g., Blain et al. 1999b, 1999c; Rowan-Robinson 2001; Xu et al. 2001). The CMD trend can be understood naturally in terms of luminosity evolution: more luminous objects occur at higher red-

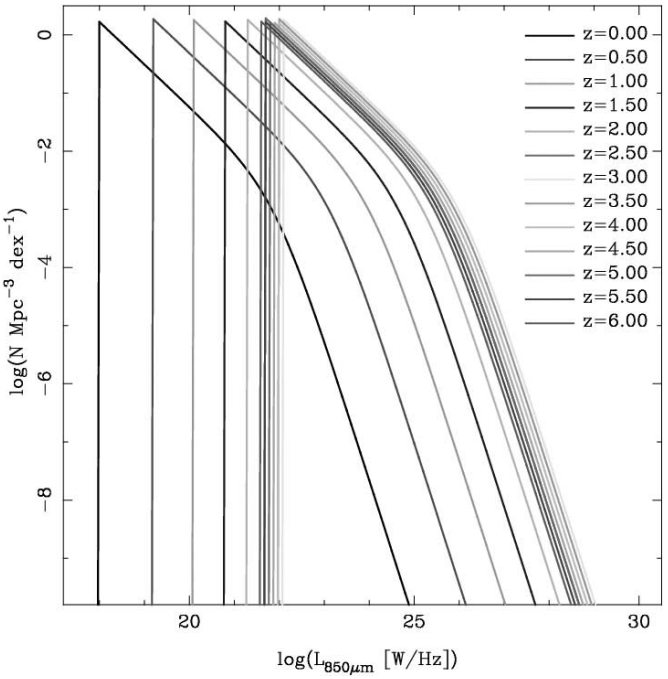

FIG. 5.—Luminosity functions adopted in our Monte Carlo models are presented, taking the form of the local *IRAS* 60 μm function (Saunders et al. 1990) mapped to 850 μm using the best-fitted dust temperature and emissivity from Dunne et al. (2000a). Evolution is pure luminosity, taking the form $(1+z)^4$, consistent with the Blain et al. (1999a) modeling results. Beyond $z = 3$, the evolution falls with a form $(1+z)^{-4}$. Lines are color coded by redshift as noted in the figure. Note that the truncation of the function at low luminosities is irrelevant for the flux densities probed by SCUBA.

shifts, thus leaving the lower right corner largely empty. We therefore turn to Monte Carlo simulations of pure luminosity evolution pictures, similar to the models of the above authors.

We must first consider carefully which local luminosity function to adopt. While many authors have adopted a local *IRAS* 60 μm luminosity function, Dunne et al. (2000a) have recently attempted to construct an 850 μm luminosity function directly from SCUBA measurements of the *IRAS*-BGS. Given that the bright end of the Dunne et al. function is still highly uncertain, we follow the lead of the previous modelers and work from the *IRAS* 60 μm function as presented in Saunders et al. (1990). We *K*-correct to 850 μm with a single temperature graybody spectrum to match as closely as possible the Dunne et al. measurements at 850 μm (using $T_d = 36$, $\beta = 1.3$).

We evolve the local luminosity function using $\Phi(L,\nu) = \Phi_0\left[L/g(z), \nu(1+z)\right]$. Our evolution function has a power-law peak, $g(z) = (1+z)^4$ out to $z = 3$ (the consensus of the median redshift for SCUBA sources suggested by Archibald et al. 2001; Smail et al. 2000; Dunlop et al. 2001; Scott et al. 2001). Beyond $z = 3$, the function drops again as $g(z) = (1+z)^{-4}$. This power-law index is chosen based on evolutionary models fitted to both optical and submillimeter wavelength data (Blain et al. 1999b, 1999c). To retain the pure luminosity evolution, we truncate the evolved functions so that they integrate to identical numbers of sources per comoving volume, as depicted in Figure 5.

We can then incorporate this luminosity evolution into our Monte Carlo models. We first introduce our luminosity evolution models into the CMD, without the radio/far-IR scatter for clarity (Fig. 6*a*). To illustrate the total sample and the effect of radio preselection, we show all sources but change the symbol size for the sources we can detect (large) and those that fall below our radio sensitivity (small). Again, sources are color-coded by redshift. We now find a scenario which is consistent with the source distribution of our observed CMD, while simultaneously fitting the submillimeter through far-IR counts and backgrounds. When we bring in the radio/far-IR scatter (Fig. 6*b*), we see that the apparent selection bias effect is even larger than in our previous model (Fig. 4), scattering sources into the region that lies above the redshift for which a suitably scaled Arp 220 SED would be detectable.

The reasonable match of this model with our measured CMD additionally suggests that there may be very high-redshift ($z \gtrsim 3$) sources in our OFRS SCUBA sample. However, consideration of the radio-undetected sources in the CMD plane indicates that the maximum luminosity for which we detect sources in the submillimeter and radio represents the peak in the adopted evolution function; sources lying at higher redshifts are necessarily less submillimeter luminous. Our present model represents the maximum amount of luminosity evolution that can be accommodated in such a peak model using the 50 K SED template without overproducing the 850 μm counts (effectively the far-IR background). With cooler dust temperatures, less severe luminosity evolution is able to reproduce our observed CMD.

6. SELECTION FUNCTION AND MODELS

6.1. *The Radio Selection Function*

Having reproduced our observed CMD data set with a scenario consistent with galaxy counts at a variety of far-IR and submillimeter wavelengths, we are now able to better understand our radio selection function relative to the modeled CMDs.

We can take our model and derive predicted versus measured counts (Fig. 7) and redshift distributions (Fig. 8). With our adopted scatter of 0.2 dex in the far-IR/radio correlation, we recover a large percentage of the submillimeter counts brighter than 10 mJy, falling to a 50% recovery rate by $\sim$5 mJy. This appears to be less than the recovery rate quoted in BCR and C01. A simple explanation for this discrepancy is that our Monte Carlo model gives sources with an infinite effective signal-to-noise ratio, while the actual data at the $\sim$5 mJy level is barely 3 σ significance. The steep luminosity function therefore results in a large Eddington bias, scattering many $\sim$2 σ sources into our detected catalog and making up an apparent excess of source counts in the $\sim$5 mJy bin.

Our modeling results have demonstrated that a simplistic estimate of the radio preselection function based on redshifting a single ULIRG falls short of the true picture. Considering the entire population of IR-luminous sources evolving in one of several plausible scenarios consistent with our CMD and the 850 μm counts, it appears that higher redshift sources will scatter into our detection window. Such high-z objects appear to comprise a significant fraction of our brightest sources, consisting of $\sim$20% of the $S_{850} > 10$ mJy detections. Our analysis of the Monte Carlo modeled source count and redshift distribution

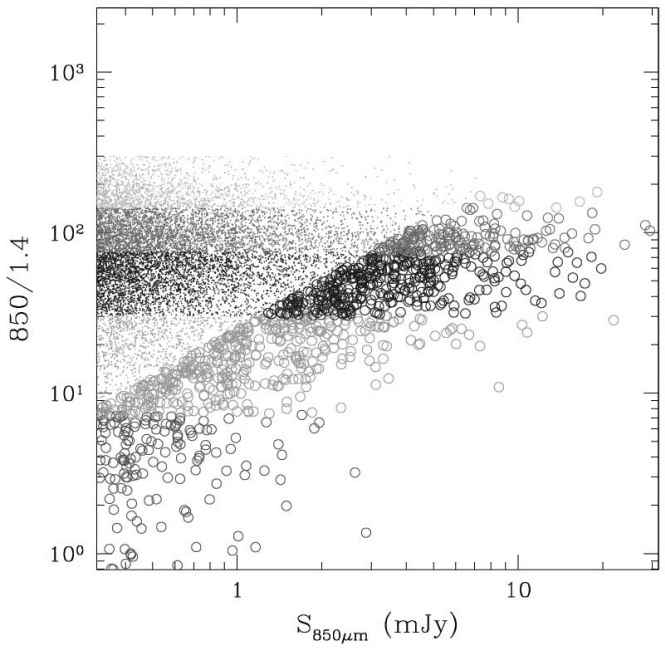

FIG. 6*a*

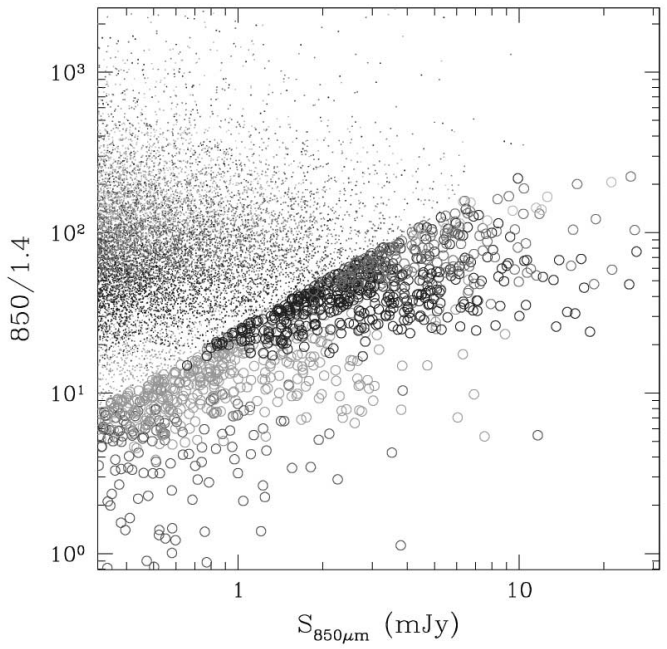

FIG. 6*b*

FIG. 6.—Monte Carlo models including luminosity evolution. (*a*) Simulation of the 850 μm/1.4 GHz CMD but without the submillimeter/radio scatter for clarity. For illustration of the total sample and the effect of radio preselection, we show all sources, but those we can detect have larger symbols. The distribution of detectable sources is qualitatively similar to our observed CMD. Redshifts are color-coded by gray scale as in previous graphs, with bands indicating $z < 1$, $z = 1$–2, $z = 2$–3, $z = 3$–4, and $z > 4$. (*b*) Scatter in the submillimeter/radio relation is now added. The source density for $S_{850} > 5$ mJy matches that of our observed CMD.

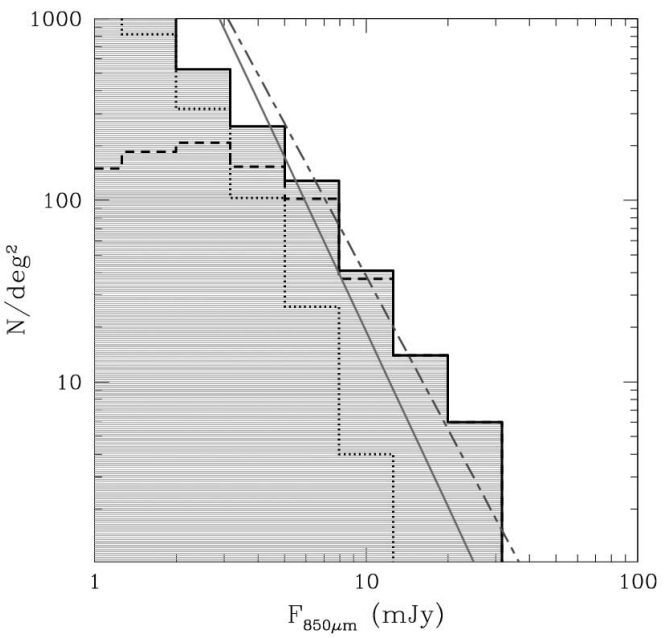

FIG. 7*a*

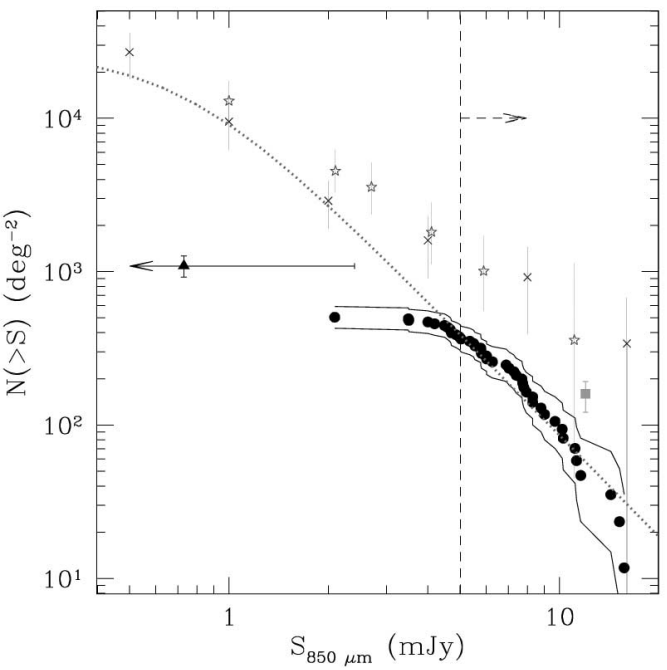

FIG. 7*b*

FIG. 7.—(*a*) Differential source counts extracted from our Monte Carlo simulations. By binning the sources from our CMD as a function of S_{850}, we can recover the total source counts as well as the fraction detected in the radio. The solid line represents the power-law fit to the blank field submillimeter source counts (Barger et al. 1999), while the dashed line represents a fit to the bright end of the lensed counts of Blain et al. (1999) and Chapman et al. (2002c). The histograms represent the total modeled counts (*solid*), the radio-detected counts (*dashed*), and the radio-undetected counts (*dotted*). With our adopted scatter of 0.2 dex in the submillimeter/radio correlation, we recover a large percentage of the submillimeter counts brighter than 10 mJy, falling to a 50% recovery rate by $\sim$5 mJy. (*b*) Integrated source counts estimated from our OFRS sample, shown by filled symbols, with estimated error band. Also plotted is the fit to blank field submillimeter survey counts of Barger et al. (1999) and Eales et al. (2000), shown by the dotted line, and the lensing amplified survey counts of Blain et al. (1999) and Chapman et al. (2002c), shown as crosses and stars, respectively. A recent measurement in the extended HDF region for sources brighter than 12 mJy is shown by the square. The fraction of sources recovered is clearly high.

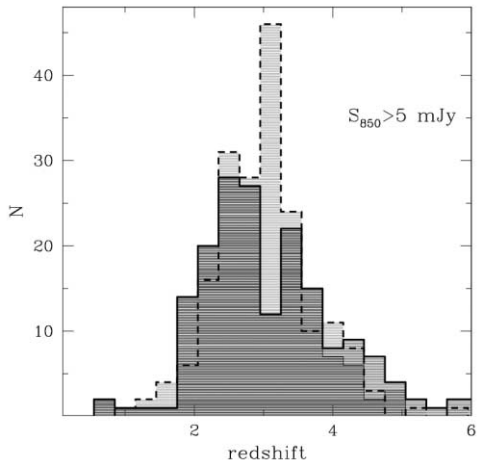

FIG. 8*a*

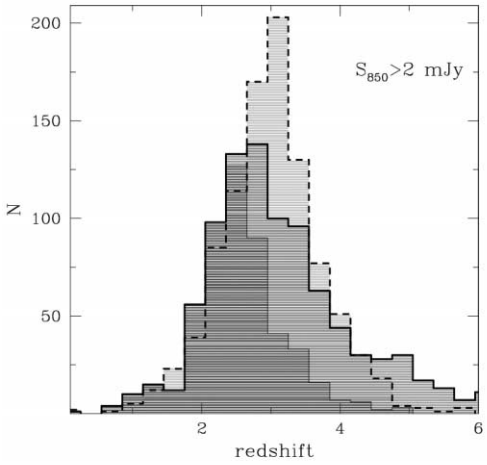

FIG. 8*b*

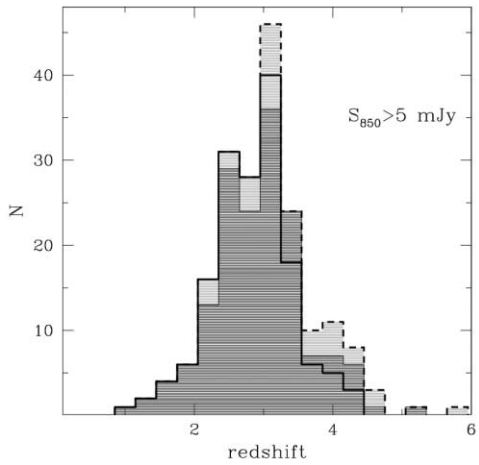

FIG. 8*c*

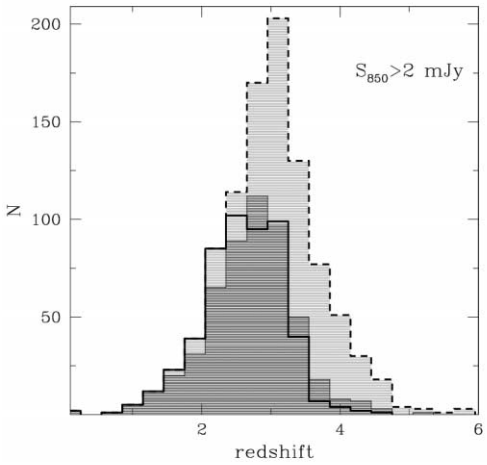

FIG. 8*d*

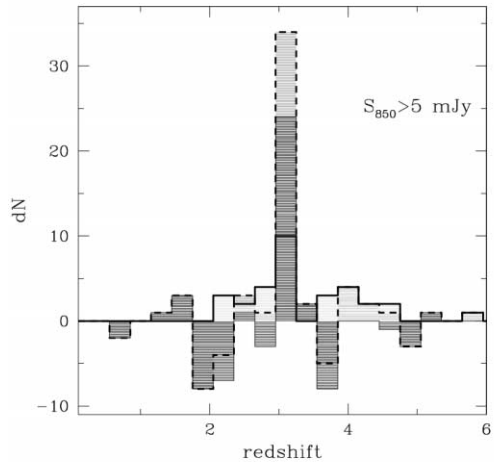

FIG. 8*e*

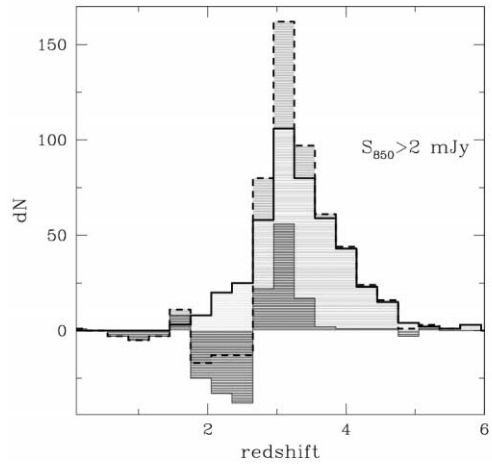

FIG. 8*f*

FIG. 8.—(*a–b*) Modeled redshift distributions extracted from our Monte Carlo simulations. Dashed lines represent the input redshift distribution of the sources, while the distribution as measured from the 850 μm/1.4 GHz ratio is plotted in dark histogram (*solid lines*). The shaded inset in the latter case represents the fraction of sources recovered from the radio preselection. The distribution measured from the 850 μm/1.4 GHz (including 0.2 dex scatter) is flattened and also broader than the true distribution. There is an excess of sources at lower redshift and also an excess of high-z sources arising simply from the intrinsic scatter in the 850 μm/1.4 GHz relation, which broadens the peak in our adopted evolution function. (*c–d*) Actual redshift distribution recovered by the radio selection (*solid histogram*) compared to the recovery in the absence of scatter in the far-IR/radio relation. In our 5 mJy flux cut, we recover an excess of sources for all $z > 3$, but recover a deficit of sources from $2 < z < 3$. Our radio-selected survey is therefore less complete at $2 < z < 3$ than we would have naively expected. (*e–f*) Residuals as an estimate of the errors involved in both the intrinsic radio selection and the 850 μm/1.4 GHz estimator. *Dashed line*: Residuals of the radio-detected sources with a 850 μm/1.4 GHz estimated redshift distribution compared with the input distribution. *Solid line*: True redshifts of radio-selected sources relative to the total distribution. *Light solid line*:Difference in the 850 μm/1.4 GHz estimated redshift from the true redshift distribution for the radio-selected sources alone.

recovery therefore suggests that we look at direct comparison with the measured blank-field submillimeter properties presented in BCR, C01, and Chapman et al. (2002, in preparation).

In Figure 7*b*, we plot the integrated source counts estimated from our optically faint radio source sample (*filled symbols with error band*). A fit to the blank-field submillimeter survey counts from BCR and Eales et al. (2000) are also shown by the dotted line and the cluster lensing survey counts of Blain et al. (1999a) and Chapman et al. (2002c) by crosses and stars, respectively. The effective volume of our survey is difficult to estimate, as the radio sensitivity falls off with radius from the field center. This issue has been quantified carefully in C01 (and will be discussed further in Chapman et al. 2002, in preparation). Since objects were chosen randomly, we use the visibility function to construct the count, as discussed in these papers.

The fraction of sources recovered is clearly high, although the brighter counts are still not very well constrained. While the $\sim$2 mJy counts are well determined to be 3000–4000 deg^{-2} brighter than 5 mJy, it is not clear how steeply the count falls. A recent measurement from Borys et al. (2001) for sources brighter than 12 mJy in the extended Hubble Deep Field is also plotted with a square. This suggests our OFRS recovery rate is about 60%.

Our modeling analysis lead us to a count recovery rate perhaps as high as 70% in the absence of large-scale structure effects. This seems plausible, both from the direct analysis of the counts comparison (Fig. 7*b*) and from the sources which we know to be missing from the OFRS preselection: the $\sim$15% optically brighter sources at all redshifts, and the remaining sources at redshifts too high to be detected in the radio. This is also in agreement with the direct comparisons of blank-field SCUBA surveys with those sources recovered in the radio from the same fields (Borys et al. 2001; Smail et al. 2001; C01). At the faint end of the counts (Fig. 7*b*), our preselected sources appear to fall significantly short of the full source counts. This was already evident in our modeling of the recovery rate (Fig. 7*a*), where only $\sim$10% were detected at the current radio depths by $S_{850} = 1$ mJy.

In Figure 8, we focus on the redshift information gleaned from the 850 μm/1.4 GHz estimators compared to the true distribution. We take two flux cuts on the modeled 850 μm data and overplot the true redshift distribution (*dashed histogram*) on that obtained by directly applying the 850 μm/1.4 GHz redshift estimator to the total population (*solid histogram*) and the radio-detected subpopulation (*inset histogram*). Figure 8*a* depicts a 5 mJy cut, corresponding roughly to the sensitivity of our SCUBA OFRS survey, while Figure 8*b* presents a 2 mJy cut comparable to the deepest observations obtainable with SCUBA. Clearly in the absence of 850 μm/1.4 GHz scatter, we recover the true redshift distribution. Introducing the scatter results in a broadening and skewing of the distribution as a result of the strong luminosity evolution adopted in our model. The radio selection (*inset histogram*) results in a bias, whereby objects at higher redshift, beyond the peak in our evolution function $g(z)$, are scattered into our radio detection window. However, these appear as an excess of $z \sim 2$ sources, having been scattered down from the large population with ever-decreasing characteristic luminosity (L^* in our luminosity functions). The excess of measured high-z sources arises simply from the intrinsic scatter in the 850 μm/1.4 GHz relation, broadening the peak in our evolution function, $g(z)$. These features must be ubiquitous in any realistic evolutionary model which rises in luminosity to a peak redshift and then declines to even higher redshifts.

These biases are quantified by comparing the actual redshift distribution recovered by the radio selection (*histogram*) to the recovery in the absence of scatter in the far-IR/radio relation (Figs. 8*c*, 8*d*). In our 5 mJy flux cut, we recover an excess of sources for all $z > 3$ but recover a deficit of sources from $2 < z < 3$. Our radio-selected survey is therefore less complete at $2 < z < 3$ than we would have naively expected based on the redshift at which Arp 220 is no longer detectable in the radio. This is important for spectroscopic follow-up of these samples (Barger et al. 1999; Ivison et al. 2000; Chapman et al. 2002b). In Figures 8*e* and 8*f*, we also plot the residuals as an estimate of the errors involved in both the intrinsic radio selection and the 850 μm/1.4 GHz estimator. The dashed line shows the residuals of those radio-detected sources with an 850 μm/1.4 GHz estimated redshift distribution compared with the true total distribution. The solid line shows the true redshifts of the radio-selected sources from the total distribution. Finally, the light solid line shows the difference in the 850 μm/1.4 GHz estimated redshift from the true redshift for the radio-selected sources alone.

In Figure 9, we plot the 850 μm/1.4 GHz estimated redshift distribution for the actual SCUBA observed sources in our sample, using the same Arp 220 template SED used in the models to derive redshifts. Utilizing a template with cooler dust would, of course, result in lower redshift estimates.

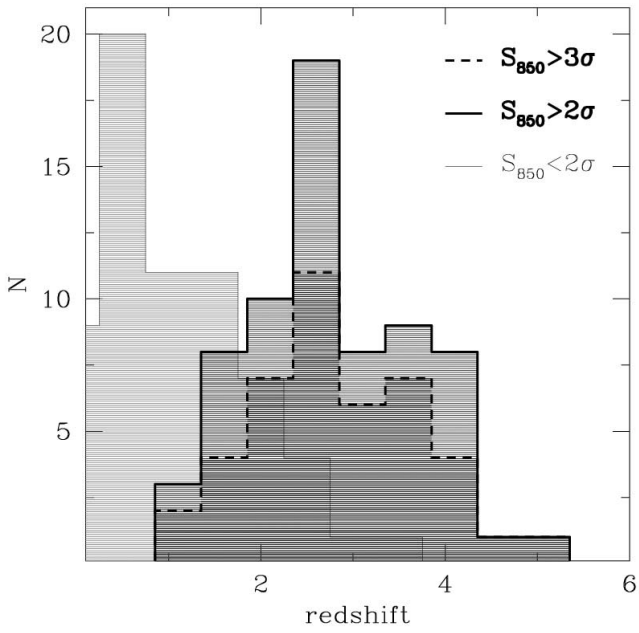

FIG. 9.—Estimated redshift distribution for SCUBA detected and undetected radio sources in our sample. We plot the histogram with a dashed line for radio sources detected in the submillimeter above a 3 σ limit. We also plot the distribution for all sources with $S_{850} > 2\ \sigma$ (*solid line, histogram*). Sources with $<2\ \sigma$ are shown with a light solid line, suggesting a tail of faint submillimeter sources extending to redshifts comparable to those spanned by the submillimeter detected sample. This 850 μm/1.4 GHz constructed redshift distribution is matched by our Monte Carlo simulations (cf. Fig. 8).

6.2. *The Optical Selection Function*

The optical selection function rejects any optically brighter submillimeter sources, which comprise >10% of the Smail et al. (2000) submillimeter survey. A constant optical limit ($I \gtrsim 24$) in the absence of evolution would select more obscured sources at lower redshifts. However, Adelberger & Steidel (2000) and Chapman et al. (2002d) have suggested that star-bursting sources appear less obscured at higher redshifts, counteracting the effect of cosmological dimming. In fact, a constant optical limit may produce the most uniform sample of sources across the $z = 1$–3 range.

The majority of the high-redshift ULIRG population, as detected by SCUBA, has been demonstrated to be optically faint, typically with $I > 24$, $K > 20$ (BCR; C01; Smail et al. 2001; Chapman et al. 2002a). Obtaining their redshift distribution is crucial for constraining their evolution and, most importantly, for placing them in their cosmological context among the hegemony of other galactic denizens (e.g., Blain et al. 1999b, 1999c). With typical magnitude of $I > 24$, however, present-generation telescopes are hard-pressed to routinely measure redshifts for such distant, faint, and highly obscured galaxies. This is particularly disappointing given that accurate redshifts are essential for obtaining CO observations of these gas-rich galaxies. The Owens Valley Radio Observatory observations presented by Frayer et al. (1998, 1999) and Chapman et al. (2002e; the SA 22 Lyα blob) of three SCUBA galaxies demonstrate the important physical information that can be obtained if accurate redshifts are available.

Fortunately, around 10% of the SCUBA-detected galaxies are unambiguously identified with relatively bright ($I < 24$) counterparts (the class II sources in the nomenclature of Ivison et al. 2000, a class which includes the two systems targeted by Frayer et al. 1998, 1999). Such galaxies are spectroscopically observable with 10 m class telescopes and so could offer one route to estimating the redshift distribution of the population as a whole. However, we first have to address the question of the relevance of these optically brighter cousins to the bulk of the SCUBA population with optically faint counterparts. Are the class II galaxies representative of the whole or are they an unrelated population, or perhaps a different episode in the evolutionary sequence?

We have shown some evidence that the optically brighter submillimeter sources may in fact be representative of the larger optically faint population (Fig. 1); the CMD reveals that optically brighter galaxies are scattered uniformly across the fainter population.

At least in part this effect may be explained, because some systems may comprise both obscured and unobscured interacting components, e.g., SMM 14011 from Ivison et al. (2000) and MMD 11 from Chapman et al. (2000, 2002f)—merging systems with the bulk of the submillimeter emission arising in one galaxy component, while the optical emission remains unobscured in an associated component. Equivalently the two components may be mixed up within a single galaxy, through patchy dust and star formation. Our radio selection of optically faint submillimeter sources is blind to these possibilities, and optically brighter sources are often located very nearby the radio position. In other cases, the galaxy may simply have substantial outflows which have expelled dust along preferred viewing directions, allowing a view through the veil.

7. THE 450 μm DETECTIONS AND THE COLOR-COLOR RELATION

Many of our sources are also detected at 450 μm, which allows for the possibility of improving the constraints on evolutionary properties for the sample. We have extracted 450 μm flux densities from the models of Figure 6 and plotted CMD and color-color diagrams in Figure 10 along with the 850 μm/radio CMD (reproduced without the confusion of sources falling beneath our radio limit). In this figure, the redshifts of the sources are mapped onto a continuous color code, represented by the bar in Figure 10.

While some of the sources are only marginally detected at 450 μm, the firm detections obtained at 850 μm and at 1.4 GHz lend support to their reality. We focus on the 19 sources with 450 μm flux detected at greater than 2 σ. These data are presented in Figure 11, where we plot both a 450 μm/850 μm CMD and a 450 μm/850 μm versus 850 μm/1.4 GHz color-color diagram. The envelopes of our Monte Carlo models are shown as dashed lines. For comparison, we also plot the five sources from the Smail et al. (2001) sample detected at 450 μm and the single source from Eales et al. (2000) by triangles and squares, respectively. The average (inverse variance weighted) signal at 450 μm of the 850 μm detected sources is 34 ± 6 mJy, consistent with a population with median $z = 3$ and our adopted dust parameters.

An additional consideration for 450 μm observations is the increased instability in the sky opacity at this shorter wavelength and the larger effect of extinction corrections as a consequence, leading to possibly larger flux uncertainties than naively estimated. The importance of such effects was discussed recently by Dunne & Eales (2001) for a sample of local galaxies measured at 450 μm. We obtained calibration maps for our data at 6 hr intervals on average, and the data were all taken near the middle of the night, where the measured gains at 450 μm are far more stable than at the extremities of the night. While the absolute calibration is therefore not necessarily the dominant error on our measured flux densities, the current inability to measure atmospheric opacity rapidly during observations precludes calibrating the data to better than 20%, and we adopt this as our nominal calibration error.

Recall that locally (§ 4), the luminous IR sources have a relatively tight 450 μm/850 μm correlation but a much larger scatter in 100 μm/850 μm and 60 μm/850 μm, the latter two being closer in rest wavelength to 450 μm in our highest redshift SCUBA sources. Therefore, the relatively flat relation of 450 μm/850 μm with 850 μm flux observed for our OFRS SCUBA observations is suggestive of a sample which is relatively uniform in dust properties. The Smail et al. (2001) sources have among the lowest 450 μm/850 μm ratios, which could be consistent with redshift effects dominating their submillimeter ratios. Our selection bias to lower redshift sources is much stronger than in their blank-field survey due to the negative submillimeter K-correction. However, the large error bar on our measurements and the associated strong Eddington (noise) bias from selecting all sources with $S_{450} > 2\sigma$ is also likely to be a factor. The correlation of 850 μm to 1.4 GHz fluxes, coupled with the skewed detection of higher redshift sources from the Eddington bias, results in an even tighter relation in the 450 μm/850 μm versus 850 μm/1.4 GHz color-color space.

If the higher redshift sources are the most luminous, as suggested by the correlation in 850 μm versus 1.4 GHz

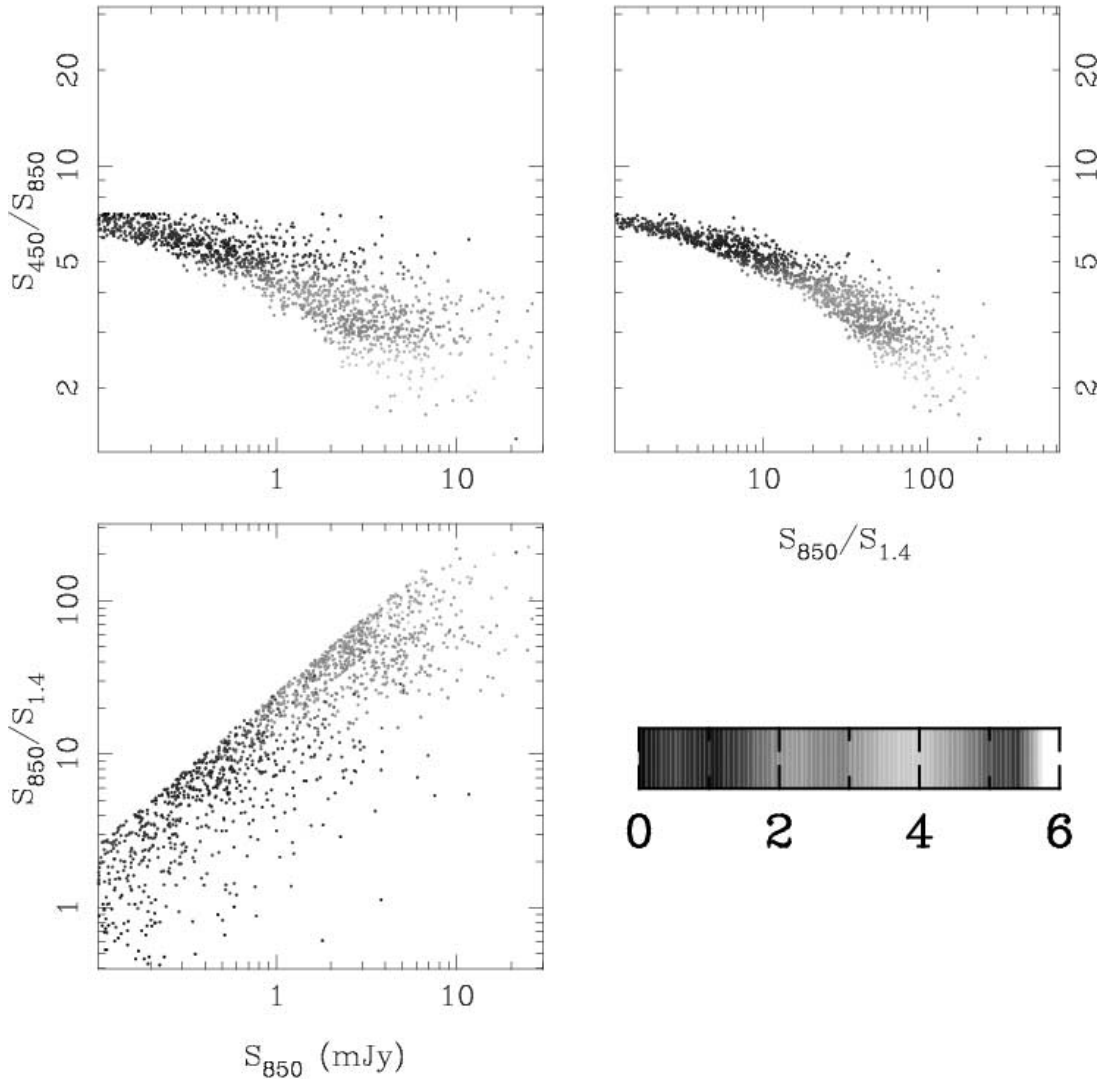

FIG. 10.—450 μm band estimates can be extracted directly from our models, which effectively use a single dust temperature of 50 K with an emissivity of $\beta = 1.5$. The model sources are color coded by redshift as indicated on the bar at lower right. The upper left plot is the S_{450}/S_{850} vs. S_{850} CMD. The main variable affecting the 450 μm/850 μm ratio is the redshift, higher redshift sources having lower ratios. The upper right plot shows the S_{450}/S_{850} vs. $S_{850}/S_{1.4}$ color-color diagram, which appears similar to the CMD, although somewhat tighter as a result of the relation between $S_{850}/S_{1.4}$ and S_{850}, which we plot in the lower left panel.

fluxes, we expect a smaller 450 μm/850 μm with increasing 850 μm flux, a result of the increasing redshift. However, we also expect brighter sources to have hotter dust based on the local *IRAS* correlation, resulting in a larger 450 μm/850 μm ratio with increasing 850 μm flux. These two effects will therefore partially cancel in the 450 μm/850 μm versus 850 μm CMD, resulting in a flat relation.

A scenario with no variation in dust properties or luminosity evolution could also produce such a flat relation. The spread in 450 μm/850 μm would then be simply a result of the redshift distribution of objects with identical dust properties. However, the radio/submillimeter correlation introduces either luminosity evolution or dust correlation with luminosity. The flat relation must therefore be the result of some intrinsic property.

Our current data do not allow robust constraints on situations where either the dust properties evolve with redshift (e.g., temperature increasing with redshift) or the population has a larger spread in dust properties with increasing redshift. While the conditions were generally rather poor at 450 μm during our JCMT runs, the 850 μm detected sources are mostly luminous enough to be detectable with SCUBA at 450 μm under more favorable conditions. Better 450 μm data would certainly improve the constraints on models.

8. DISCUSSION

8.1. *Density Evolution and the Nature of Submillimeter Galaxies*

Studies of hierarchical galaxy formation pictures suggest that significant density evolution must occur (e.g., Cole et al. 2000; Blain et al. 1999c). Successful multiwavelength evolutionary scenarios have already been explored within this paradigm (e.g., Blain et al. 1999c). However, the question for our purposes concerns the significance of merging subfragments for the 15″ scales probed by the SCUBA beam. The SCUBA sources seem likely to trace the merger

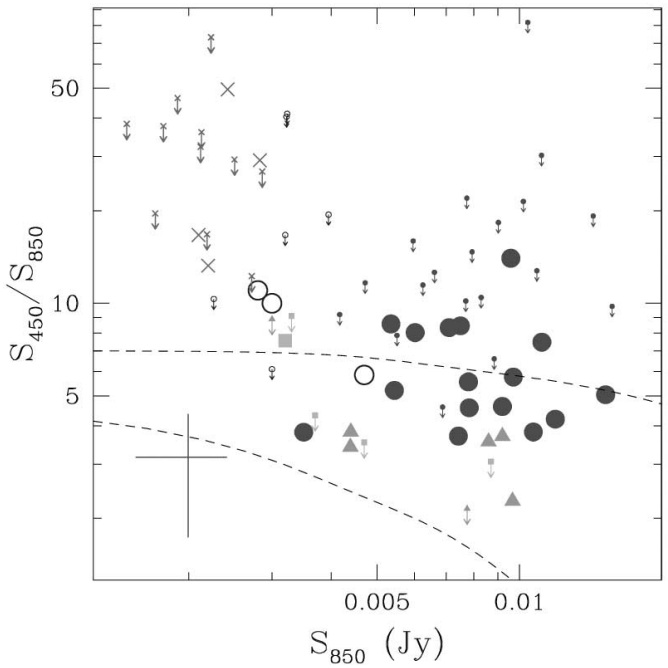

FIG. 11*a*

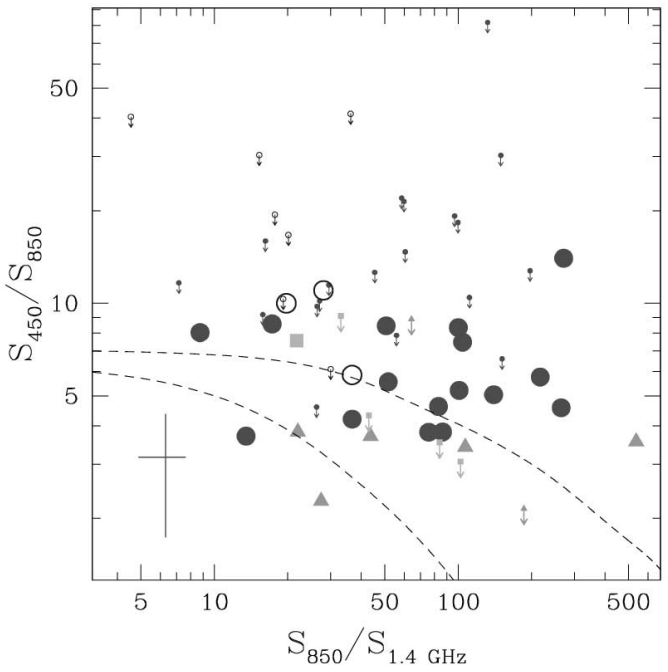

FIG. 11*b*

FIG. 11.—Nineteen sources 450 μm flux density detected at $>2\,\sigma$. A representative error bar for our detected sample is displayed in the lower left corner. (*a*) S_{450}/S_{850} vs. S_{850} CMD, with all sources undetected at 450 μm presented as $2\,\sigma$ upper limits. Dashed lines indicate the envelope of our models. (*b*) S_{450}/S_{850} vs. $S_{850}/S_{1.4}$ color-color diagram. The results from our single (50 K) dust temperature model are overlaid as an envelope defining the region of detected sources from Fig. 10. The measured sources are consistent within 1σ of the envelope, but on average have a higher 450 μm/850 μm value. The sources from the Smail et al. (2001) catalog (*triangles*) and the source from Eales et al. (2000, *square*) lie near the lowest values of 450 μm/850 μm that we find from the OFRS sample (*solid circles*). Given the relation between $S_{850}/S_{1.4}$ and S_{850}, the color-color plot is similar to the CMD. The source positions are rearranged in the color-color plot, suggesting that the 850 μm luminosities are somewhat independent of redshift.

events themselves rather than the fragments coming together before merging (and perhaps surviving afterwards without any significant far-IR emission). Therefore, pure luminosity evolution is not necessarily a poor model for the bright end of the SCUBA counts. The situation described above for optically bright versus faint SCUBA sources is also relevant here; luminous sources may sometimes pair with a merging optically bright source, or a snapshot in the merger sequence may have optically luminous and dust-enshrouded parts.

Number evolution, however, is not only driven by merging. The SCUBA bright population (if driven by star formation) may represent a transitory stage in a galaxy's evolution, possibly related to the AGN phenomenon (e.g., Lewis & Chapman 2002; Archibald et al. 2001).

The effect of currently fashionable flat, $\Lambda \simeq 0.7$ cosmologies is to make the situation worse by introducing a slope to the color-magnitude plot, which also has to be countered with luminosity evolution. This would require even stronger evolution than the $(1+z)^4$ adopted in our present study, assuming the characteristic dust temperature of the sources is unchanged. An alternative would be to bring in an additional density evolution component. We have certainly not demonstrated that our particular model is a unique solution. But it seems that strong luminosity evolution is a requirement of a successful model.

8.2. *The Nature of the Sources and Future Work*

The fainter submillimeter sources, marginally detected at 2–6 mJy, clearly follow the observed and modeled CMD trend. This suggests that pursuing these candidate fainter sources with deeper SCUBA integrations could yield significant detections, providing a valuable lever arm in luminosity for modeling the evolutionary properties of the sample. The most luminous $z \sim 3$ Lyman-break galaxies are known to emit at the 1–2 mJy level (Chapman et al. 2000, 2002d; Peacock et al. 2000), so their $z = 1$–2 counterparts probably contribute some fraction of these fainter submillimeter sources. This is consistent with the high star formation rate deduced by Steidel et al. (1999), who apply a large dust correction to their results.

Note that whether or not a source has an AGN may not have a tremendous influence on its position in the CMD, especially if the energetics are still dominated by star formation. It has also been pointed out many times (e.g., Sanders 2001) that AGNs and starbursts are both related to merging, and so AGNs and starbursts could be the same objects caught at different evolutionary phases. In that case, many of the correlations between fluxes at different wavelengths may continue to hold, at least for weak AGNs.

Ho & Peng (2001) have investigated the strength of the radio synchrotron emission from Seyferts and LINERs locally. The radio-loud AGN effect on the CMD is to lower points (brighten the radio), which cannot easily be compensated for by other properties—dust temperature, for example. This suggests further that it is unlikely that radio-loud AGNs dominate the submillimeter luminous sources. One source from Smail et al. (2001) which has been identified with an AGN component inhabits the lower cutoff region of the CMD, suggesting that this region may in general be inhabited by those submillimeter sources with stronger

AGN components (a stronger AGN radio source). However, SMM 14011 (Ivison et al. 2000), which has been confirmed spectroscopically as a star-forming galaxy, also inhabits this region, and we can draw no firm conclusions that AGNs show their presence in any obvious manner in our CMD or color-color diagnostics.

Future work identifying the actual counterparts at multiple optical wavelengths, as well as obtaining a larger sample of radio sources with SCUBA measurements (both optically bright and faint), will lead to substantial refinement of our understanding of these issues. Higher spatial resolution *HST* observations may also elucidate the morphologies of the sources, allowing an understanding of how the radio/submillimeter emission is traced by the optical, and where the heart of the far-IR energy is generated in high-redshift objects. Deeper submillimeter observations of the submillimeter faint radio sources will allow us to place them in context relative to the submillimeter bright radio sources.

9. CONCLUSIONS

We have presented a large sample (55) of submillimeter sources with radio and optical counterparts. We observe a correlation between the submillimeter flux and the submillimeter/radio, which implies that higher redshift sources must be more luminous. Local correlations in the radio/submillimeter/far-IR properties of luminous infrared galaxies provide a benchmark for assessing the trends observed in our higher redshift analogs. In particular, the effects of dust temperature on our evolutionary scenario can be directly assessed. Using a Monte Carlo approach to model the evolution of the IR luminous galaxies, we are able to simultaneously represent the CMD, counts, and submillimeter/radio-implied redshift distribution for our observed sample. Our models are not unique but indicate some general features which any successful model must possess; in particular, this strong luminosity evolution.

The selection function from submillimeter follow-up to optically faint radio can be better understood in relation to our Monte Carlo models. There are inherent biases in the technique beyond that expected from a naive redshifting of the Arp 220 SED out to redshifts where it is no longer detectable in the radio. The combination of radio/far-IR scatter and the necessary rise and fall in the evolution function results in a bias in the selection of sources (if we were able to obtain spectroscopic redshifts for the entire sample). We uncover an excess of high-redshift sources and lose some of the lower redshift sources that would otherwise be present in our selection window. In the absence of spectroscopic redshifts, the reconstruction of the redshift distribution is broadened and weighted toward lower redshifts. The few optically bright submillimeter sources in our sample are distributed uniformly throughout the CMD with no preferred locus. This suggests that spectroscopic follow-up of the optically brighter population may provide a reasonable approximation to the true redshift distribution.

This redshift distortion presents the possibility of a population of very high-redshift ($z > 3$) star-forming galaxies being detected with our radio selection approach. With current radio flux limits, the required luminosities are too large to be included in our sample for $z > 5$ under the assumptions of our present model.

A subsample of 25 sources are marginally detected in the 450 μm band. When compared to local *IRAS* galaxies, these suggest a similar range in dust properties to local ULIRGs, possibly with somewhat hotter or more emissive dust.

We thank the staff of the JCMT for their assistance with the observations. The referee, C. Carilli, has helped us to improve the final version of this paper. A special thanks to R. Ivison, I. Smail, A. Blain, and L. Dunne for helpful discussions of this work. We gratefully acknowledge support from NASA through *Hubble Space Telescope* grant 9174.1 (SCC) and Hubble Fellowship grant HF-01117.01-A (E. A. R.) awarded by the Space Telescope Science Institute, which is operated by the Association of Universities for Research in Astronomy, Inc., for NASA under contract NAS 5-26555. G. F. L. thanks the Australian Nuclear Science and Technology Organization (ANSTO) for financial support. D. S. and C. B. are supported by the Natural Sciences and Engineering Research Council of Canada.

REFERENCES

Adelberger, K., & Steidel, C. 2000, AJ, 119, 2556
Archibald, E., et al. 2001, MNRAS, 323, 417
Barger, A., Cowie, L., Mushotzsky, R., & Richards, E. 2001a, AJ, 121, 662
Barger, A., Cowie, L., Richards, E. 2000a, AJ, 119, 2092 (BCR)
Barger, A., et al. 2001, AJ, 122, 2177
———. 2001, ApJ, 560, L23
———. 1999, AJ, 117, 2656
Bertoldi, F., et al. 2000, A&A, 360, 92
Blain, A. 2000, MNRAS, 309, 955
Blain, A., et al. 1999a, ApJ, 512, L87
———. 1999b, MNRAS, 302, 632
———. 1999c, MNRAS, 309, 715
———. 1999d, MNRAS, 309, 955
Borys, C., Chapman, S. C., Scott, D., & Halpern, M. 2002, MNRAS, 330, 63
Carilli, C., & Yun, M. 2000, ApJ, 530, 618
———. 1999, ApJ, 5130, L13
Chapman, S. C., et al. 2002a, MNRAS, submitted
———. 2002b, ApJL, submitted
Chapman, S. C., Richards, E., Lewis, G. F., Wilson, G., & Barger, A. 2001a, ApJ, 548, L147 (C01)
Chapman, S. C., Scott, D., Borys, C., & Fahlman, G. 2002c, MNRAS, 330, 92
Chapman, S. C., et al. 2000, MNRAS, 319, 318
Cole, S., et al. 2000, MNRAS, 319, 168
Condon, J. 1992, ARA&A, 30, 575
Condon, J., Helou, G., Sanders, D., & Soifer, B. 1996, ApJS, 103, 81
Dale, D., et al. 2001a, ApJ, 549, 215
———. 2001b, ApJ, submitted
Dunlop, J. 2001, in Proc. FIRSED 2000, The Spectral Energy Distributions of Far-Infrared Galaxies, ed. I. M. van Bemmel, B. Wilkes, & P. Barthel (Amsterdam: Elsevier)
Dunne, L., et al. 2000a, MNRAS, 319, 813
———. 2000b, MNRAS, 315, 115
Dunne, L., & Eales, S. 2001, MNRAS, 327, 697
Eales, S., et al. 2000, AJ, 120, 2244
Fixsen, D.J., et al. 1998, ApJ, 508, 123
Fomalont, E., et al. 2002, ApJ, in press
Frayer, D., et al. 1999, ApJ, 514, L13
———. 1998, ApJ, 506, L7
Helou, P., et al. 1985, ApJ, 440, 35
Ho, L., & Peng, C. Y. 2001, ApJ, 555, 650
Holland, W., et al. 1999, MNRAS, 303, 659
Ivison, R., et al. 2000, MNRAS, 315, 209
Lewis, G., & Chapman, S. C., 2002, MNRAS, in press
Peacock, J., et al. 2000, MNRAS, 318, 535
Puget, J.-L., et al. 1996, A&A, 308, L5
Richards, E. 2000, ApJ, 533, 611
Richards, E., et al. 1999, ApJ, 526, L73
Rowan-Robinson, M. 2001, ApJ, 549, 745
Sanders, D. B. 2001, in IAU Colloq. 184, AGN Surveys, ed. R. F. Green, E. Y. Khachikian, & D. B. Sanders (San Francisco: ASP), 29

Saunders, R., et al. 1990, MNRAS, 257, 425
Scott, S., et al. 2001, MNRAS, submitted (astro-ph/0107446)
Smail, I., et al. 2002, ApJ, in press
———. 2000, ApJ, 528, 612
Smail, I., Ivison, R. J., & Blain, A. W. 1997, ApJ, 490, L5
Steidel, C., Adelberger, K., Giavalisco, M., Dickinson, M., & Pettini, M. 1999, ApJ, 519, 1
Xu, C., et al. 2001, ApJ, 562, 179
Yun, M., Reddy, N., & Condon, J. 2001, ApJ, 554, 803